Arabian Journal of Chemistry (2021) **14**, 103440

King Saud University

Arabian Journal of Chemistry

www.ksu.edu.sa
www.sciencedirect.com

ORIGINAL ARTICLE

The preparation of ionic liquid based iron phosphate/CNTs composite via microwave radiation for hydrogen evolution reaction and oxygen evolution reaction

Yanping Chen [a], Qichao Zhao [b], Yanling Yao [c,*], Tianhao Li [a,d,*]

[a] *Chongqing Key Laboratory for Advanced Materials and Technologies of Clean Energy, School for Materials and Energy, Southwest University, Chongqing 400715, China*
[b] *Bureau of Hydrology, Changjiang Water Resources Commission, Wuhan 430010, China*
[c] *School of Chemistry and Materials Engineering, Huizhou University, Huizhou 516007, China*
[d] *Guangdong Provincial Key Laboratory of Advanced Energy Storage Materials, South China University of Technology, China*

Received 18 June 2021; accepted 8 September 2021
Available online 17 September 2021

KEYWORDS

Ionic liquid;
Iron phosphate;
Electrocatalyst;
Hydrogen evolution reaction;
Oxygen evolution reaction

Abstract Water electrolysis is a promising method for hydrogen production, so the preparation of low-cost and efficient electrocatalysts with a quick and simple procedure is crucial. Herein, iron phosphate ($Fe_7(PO_4)_6$) was prepared *via* microwave radiation using ionic liquid (IL) as iron and phosphorus dual-source. This method is simple and rapid, and the product can be directly used as electrocatalysts without further treatment. The experimental results show that the IL can influence the morphology and electrocatalytic performance. Moreover, the addition of carbon nanotubes (CNTs) is favorable for formation of iron phosphate nanoparticles to improve the catalytic activities. As hydrogen evolution reaction (HER) catalyst, this iron phosphate/CNTs exhibits an onset overpotential of 120 mV, Tafel slope of 32.9 mV dec^{-1}, and current densities of 10 mA cm^{-2} at overpotential of 185 mV. Then, it obtains a good activity for oxygen evolution reaction (OER) with a low onset potential of 1.48 V, Tafel slope of 73.3 mV dec^{-1}, and it only needs an overpotential of 300 mV to drive the 10 mA cm^{-2}. This bifunctional catalyst also shows good durability for HER and OER. This microwave-assisted method provides an outstanding strategy to pre-

* Corresponding authors at: Chongqing Key Laboratory for Advanced Materials and Technologies of Clean Energy, School for Materials and Energy, Southwest University, Chongqing 400715, China (T. Li).
E-mail addresses: wsmandyy@163.com (Y. Yao), til7@swu.edu.cn (T. Li).
Peer review under responsibility of King Saud University.

Production and hosting by Elsevier

https://doi.org/10.1016/j.arabjc.2021.103440

pare iron phosphate in a simple and fast process with good catalytic performance for water splitting.

1. Introduction

With the dramatic increasing of energy demand and environmental impact, numerous efforts have been conducted to develop sustainable and clean energies. Hydrogen is regarded as a promising candidate due to its eco-friendly, highly efficient energy conversion, and high energy density (Turner, 2004; Schlapbach, 2009). Water electrolysis is a simple and mature way for massive hydrogen and oxygen production without carbon emission (Coughlin, 1979). RuO_2 and Pt/C are the most widely used commercial electrocatalysts for oxygen evolution reaction (OER) and hydrogen evolution reaction (HER) in water electrolysis, respectively. Nevertheless, their high-cost and scarce-abundance limit the practical application (Yang et al., 2018; Wang et al., 2017; Sun et al., 2020). Thus, it is critical to explore some low-cost and high-efficient electrocatalysts for water splitting.

To date, transitional metal sulfides, nitrides, phosphates and phosphides have been widely studied as electrocatalysts for HER and OER since their excellent conductivity and stability, low price and high abundance (Li et al., 2020). Recently, experimental and theoretical investigations indicate that P atom can significantly decrease the Gibbs free energy of hydrogen adsorption, improving the HER performance (Callejas et al., 2015; Shi, Y., Zhang., 2016). P-defects in the catalyst can adjust the binding intensity between intermediates and catalytic sites to reduce the free-energy barrier, which is pivotal for OER process (Pu et al., 2017; Yao et al., 2018). In addition, P was oxidized to oxides and phosphates thatimprove the OER performance (Yu, et al., 2551). Thus, transitional metal phosphates can be applied as HER and OER bifunctional electrocatalyst.

In recent years, various kinds of transitional metal phosphates, including iron, cobalt, nickel and molybdenum based phosphates were surveyed as catalysts in water electrolysis (Liang et al., 2019; Zhong et al., 2017; Zhang et al., 2017). In these materials, iron phosphates are adequately studied as HER and OER electrocatalysts for large scale application due to the fact that iron is the cheapest and most abundant transition metal (Khalate et al., 2019; Zhang et al., 2017; Zhong et al., 2017). Moreover, iron phosphate possesses low toxicity and environmental impact.

In order to prepare the iron phosphate/phosphide, NaH_2PO_2, phosphorus and thrioctylphosphide are the most frequently used P sources, and different iron salts ($FeCl_3$ or $Fe(NO_3)_3$) are usually utilized as the Fe sources. However, some extra pretreatment steps for these raw materials are usually needed to obtain better catalytic performance. Moreover, conventional pyrolysis strategies are usually tedious and energy consuming. Therefore, a simple and rapid synthesis approach for iron phosphate is highly required. In this study, a microwave-assisted strategy was proposed to obtain iron phosphate-carbon nanotubes (FePO/CNTs) composite using ionic liquids (ILs) as Fe and P sources. This synthesis approach is simple and quick that can be completed with 10 min. Tetrabutylphosphonium tetrachloroferrate ($[P(C_4H_9)_4][FeCl_4]$) with CNTs was applied to obtain $Fe_7(PO_4)_6$/CNTs that showed good electrocatalytic activities and stabilities for HERand OER. As a HER catalyst, it exhibits an onset overpotential of 120 mV, Tafel slope of 32.9 mV dec^{-1}, and current densities of 10 mA cm^{-2} at overpotentials of 185 mV. Then, it obtains a good activity for OER with a low onset potential of 1.48 V, Tafel slope of 73.3 mV dec^{-1}, and it only needs an overpotential of 300 mV to drive the 10 mA cm^{-2}.

2. Experimental

2.1. Reagents

Tetrabutylphosphonium chloride ($[P(C_4H_9)_4][Cl]$), Trihexyl(tetradecyl)phosphonium chloride ($[P(C_6H_{13})_3C_{14}H_{29}][Cl]$) and iron(III) chloride hexahydrate ($FeCl_3{\cdot}6H_2O$) were obtained from Titansci Co. China. Multi-walled carbon nanotubes (CNTs) were supplied by Shenzhen Nanotech Port Ltd,Co. China.Pt/C (20 wt%) and RuO_2 were purchased from Aladdin. All other reagents were supplied by Beijing Chemicals, China. Deionized water (18 MΩ cm) obtained from a Milli-Q Plus system (Millipore) was used throughout the experiment.

2.2. Preparation of ionic liquid and iron phosphates

The synthesis of the two ionic liquids (ILs), namely tetrabutylphosphoniumtetrachloroferrate ($[P(C_4H_9)_4][FeCl_4]$) and trihexyl(tetradecyl)phosphonium tetrachloroferrate ($[P(C_6H_{13})_3C_{14}H_{29}][FeCl_4]$) followed the method described in our previous reports. The ($[P(C_4H_9)_4][FeCl_4]$) were prepared as follows (Scheme 1). Briefly, tetrabutylphosphonium chloride ($[P(C_4H_9)_4][Cl]$) reacted with iron(III) chloride hexahydrate ($FeCl_3{\cdot}6H_2O$) in an appropriate amount of methanol for 24 h at room temperature. After removing the methanol, the homogeneous mixture was dried in a vacuum at 45 °C for 24 h to obtain $[P(C_4H_9)_4][FeCl_4]$. This IL was mixed with

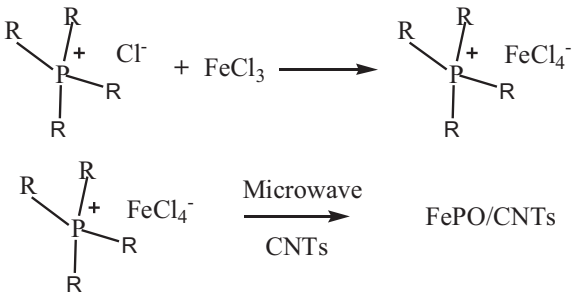

Scheme 1 Synthesis of IL and preparation of FePO/CNTs.

CNTs (IL/CNTs = 5:1, (w/w)) in an appropriate amount of methanol, and sonicated for 30 min. Then, this homogeneous product was dried in a vacuum at 45 °C for 24 h to obtain the IL4/CNTs mixture. The IL4/CNTs was then put in the microwave oven (Midea M1-201A). After 4 min of microwave radiation, iron phosphates (FePO(IL4)/CNTs) was prepared. Similarly, $[P(C_6H_{13})_3C_{14}H_{29}][Cl]$reacted with $FeCl_3{\cdot}6H_2O$ to obtain ($[P(C_6H_{13})_3C_{14}H_{29}][FeCl_4]$) that was further mixed with CNTs to get FePO(IL6)/CNTs *via* microwave for 4 min. For comparison, $[P(C_4H_9)4][FeCl_4]$ and $[P(C_6H_{13})_3C_{14}H_{29}][FeCl_4]$ directly underwent microwave radiation without adding CNTs to prepare FePO(IL4) and FePO(IL6) in the same conditions.

2.3. Electrocatalytic performance

All the electrochemical and electrocatalytic properties of the materials were systemically evaluated with an electrochemical work station (CHI-760E) using a traditional three-electrode configuration at room temperature. HER and OER were tested in 0.5 M H_2SO_4 and 1 M KOH solution, respectively. In the typical cell configuration, a saturated calomel electrode (SCE) and a graphite plate were used as the reference electrode and the counter electrode, respectively. A glassy carbon electrode (GCE, 0.126 cm^2) coated with 10 μL of 5 mg ml^{-1} catalyst solution that contains 5- wt% Nafion was used as the working electrode. Linear sweep voltammetry (LSV) was performed in the potential range of 0 to − 1 V (HER) at a scan rate of 2 mVs^{-1} and in the potential range of 0 to 1 V (OER) at a scan rate of 5 mV s^{-1} to obtain polarization curves. The electrochemical impedance spectroscopy (EIS) of electrocatalyst was recorded from 0.1 Hz to 1000 kHz, and the amplitude of current perturbation was 5 mA. The electrochemical active surface areas (ECSA) were obtained *via* cyclic voltammetry (CV) with different scanning rates. In order to reduce errors, each experiment was repeated at least three times.

2.4. Characterization

The morphology and microstructure of the catalyst were characterized by scanning electron microscopy (SEM, JSM-6510LV), transmission electron microscopy (TEM,JEM-2100) and Energy dispersive X-ray spectroscopy (EDX, INCA X-Max 250). X-ray diffraction (XRD) patterns were recorded with a RigakuD/Max 2550 diffractometer with Cu Kα radiation (λ = 1.5418 Å). X-ray photoelectron spectroscopy (XPS) measurements were performed using a Thermo Fisher ESCALAB 250Xi spectrometer with a 150 W Al Kα excitation source at 1486.6 eV.

3. Results and discussion

In this study, ionic liquid ($[P(C_4H_9)4][FeCl_4]$ or $[P(C_6H_{13})_3C_{14}H_{29}][FeCl_4]$), containing P and Fe, was utilized as iron and phosphorus sources (Scheme 2). During the microwave radiation, trialkylphosphine (TAP) was generated from phosphonium cation and $FeCl_4^-$ can be form the iron nanoparicles (Fe-NPs) (Read et al., 2016; Wang et al., 2016). TAP is the organophosphine reagent with a strong coordination interaction, which can attract Fe-NPs to form Fe-TAP complex (Pan et al., 2015). Then, P-C bond was broken to generate phosphorus. Subsequently, Fe was phosphorized to afford cobalt phosphate (FePO). Compared to the previous pyrolysis methods, this microwave method is simple and rapid, which can be finished in several minutes without any other additives.

The morphology of the as-prepared catalysts (FePO/CNTs) was observed *via* scanning electron microscopy (SEM) and transmission electron microscopy (TEM). As illustrated in Fig. 1, the SEM and TEM images of FePO(IL4)/CNTs and FePO(IL6)/CNTs manifest that iron phosphate was uniformly formed on the CNTs. The FePO(IL4)/CNTs has a snowflake-like structure, and no obvious particulate matter is visible (Fig. 1a). As shown in Fig. 1c, the TEM image of FePO (IL4)/CNTs demonstrates that iron phosphate was uniformly distributed on the CNTs like bubble. Meanwhile, SEM and TEM images of FePO(IL6)/CNTs Fig. 1b and Fig. 1d) display that iron phosphate has a sphere-shaped morphology. According to the TEM image, the particle size distribution histogram was obtained (Figure. S1 in Supplementary Material), and it indicated that the diameter of the particles is between 40 and 50 nm. These results indicated IL affects the morphology of the catalyst, and iron phosphate was enwrapped by CNTs. X-ray (EDX) spectrum (Fig.S2) indicates that Fe, P, O, and C are the main elements in the catalyst. EDS mapping results demonstrate that the Fe, P and O are homogeneously spread on the CNTs, confirming the successful synthesis of iron phosphate (Fig. S3). In order to comparison, FePO(IL4) and FePO (IL6) were also analyzed by SEM, TEM and EDS. As illustrated in Fig. S4, FePO(IL4) and FePO(IL6) have large flake morphologies, indicating bulky FePO was formed. After addition of CNTs, CNTs (solid) can disperse the IL (liquid) into small droplets to form "bucky gel" instead of homogeneous solution. Also, CNTs have a good microwave absorption performance that can transfer the heat from CNTs to IL droplets quickly. Therefore, the addition of CNTs can help to form the iron phosphate nanoparticles.

In order to investigate the crystallinity and chemical composition of the iron phosphate/CNTs, and further identify

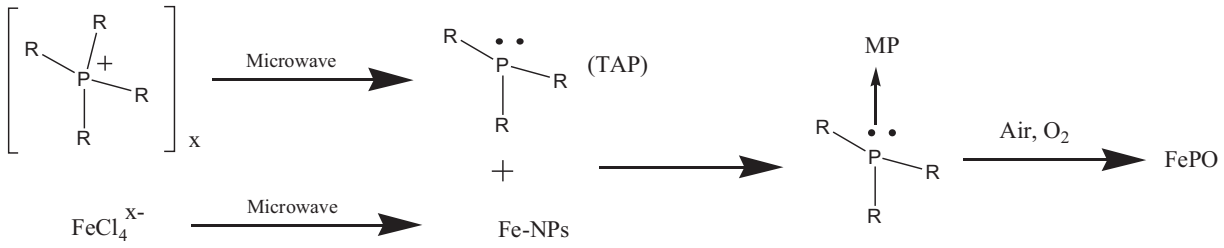

Scheme 2 Preparation process of FePO using IL.

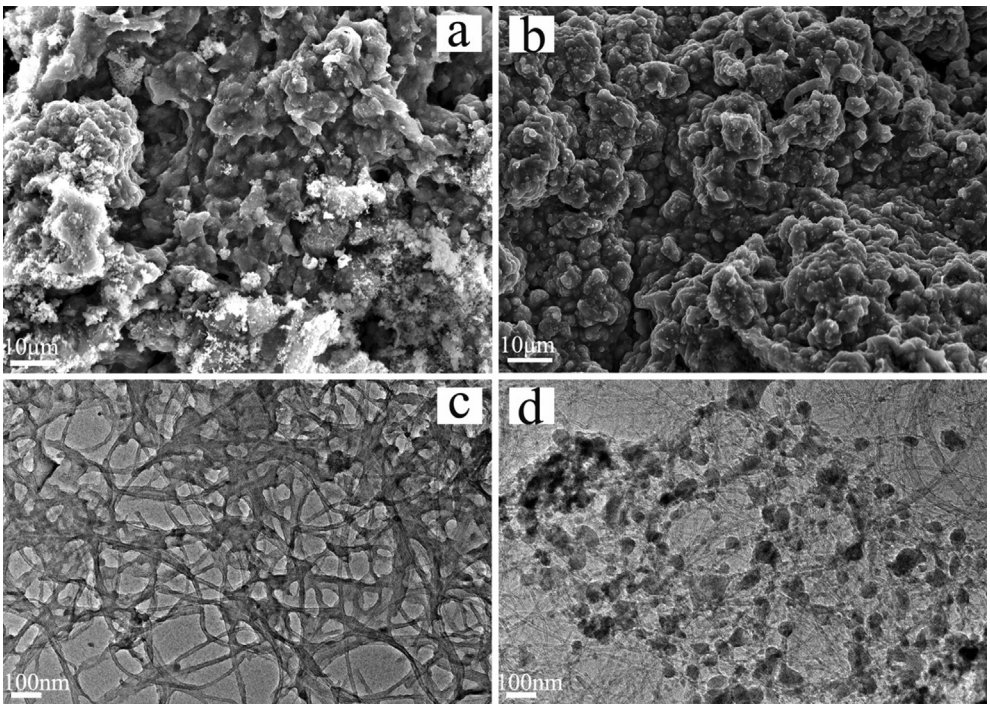

Fig. 1 **(a):** SEM image of FePO(IL4)/CNTs; **(b)**: SEM image of FePO(IL6)/CNTs; **(c)**: TEM image of FePO(IL4)/CNTs; **(d)**: TEM image of FePO(IL6)/CNTs.

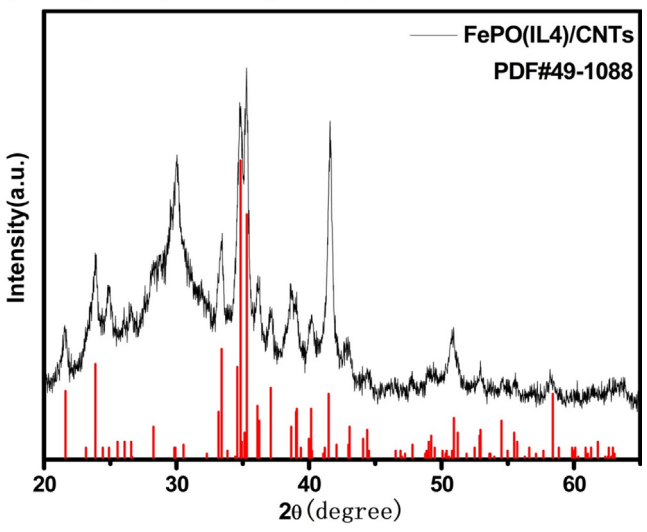

Fig. 2 XRDpattern of FePO(IL4)/CNTs.

the formation of iron phosphate, the XRD analysis was performed. As illustrated in Fig. 2, the strong peaks of XRD patterns for FePO(IL4)at 21.6, 23.8, 33.3, 34.8, 35.3, 37.0, 41.1 and 58.3° are clearly observed, which can be well matched to planes of the $Fe_7(PO_4)_6$ (PDF No.491088). The broad peaks from 26 to 31° can be attributed to the presence of CNTs and amorphous carbon generated from the carbonization of IL cation.

The bonding information of FePO(IL4)/CNTs was further studied by X-ray photoelectron spectroscopy (XPS). The FePO(IL4)/CNTs XPS spectra showed characteristic peaks of Fe2p, P2p, C1s and O1s, indicating the presence of Fe, P, O and C elements (Fig. 3a).In the Fe 2p spectrum (Fig. 3b), the characteristic peaks at 710.4 and 723.4 eV reflect the BE of $Fe^{2+}2p_{3/2}$ and $Fe^{2+}2p_{1/2}$, respectively. Moreover, the second double peaks around 712.2 and 725.3 eV correspond to$2p_{3/2}$ and $2p_{1/2}$ of Fe^{3+}, and these results confirm the coexistence of Fe^{2+} and Fe^{3+} (Wang et al., 2020 Suliman et al., 2019; Kozlyakova et al., 2018; Fan et al., 2019). The peaks 715.3 and 728.4 eV can be ascribed to the satellite peaks. The P 2p XPS spectrum is shown in Fig. 3c, and there are two peaks at the binding energies of 133.2 and 134.1 eV, corresponding to the $2p_{3/2}$ and $2p_{1/2}$ core energy levels of the phosphorus atom in the phosphate group (Yuan et al., 2016; Li et al., 2018; Xu et al., 2018). As presented in Fig. 3d, the peak appears at 531.9 eV is corresponding to O-P bonding, and the peak at 533.6 eV can be attributed to the adsorbed OH groups (Li et al., 2018; Xu et al., 2018; Yang et al., 2017).

The HER performances of FePO(IL4)/CNTs and FePO (IL6)/CNTs electrocatalysts were investigated in 0.5 MH_2SO_4. For comparison, Pt/C (20 wt%), CNTs and FePO(IL4) were also evaluated under the same conditions. As illustrated in Fig. 4a, FePO(IL4)/CNTs exhibited the best HER activity with the lowest onset overpotential of 120 mV.The FePO (IL4)/CNTs requires overpotential of 185 mV to obtain 10 mA cm^{-2}, whereas FePO(IL6)/CNTs, FePO(IL4) and CNTs need larger overpotentials to reached this current density. Furthermore, its catalytic activity is comparable with other transition metal based electrocatalysts (Table S1 in Supplementary Material). It also can be observed that the FePO (IL4) show a much lower HER activity than FePO(IL4)/CNTs, suggesting CNTs play an important role in improving HER performance. One possible reason is that CNTs can effectively disperse IL into small droplets, which helps to form

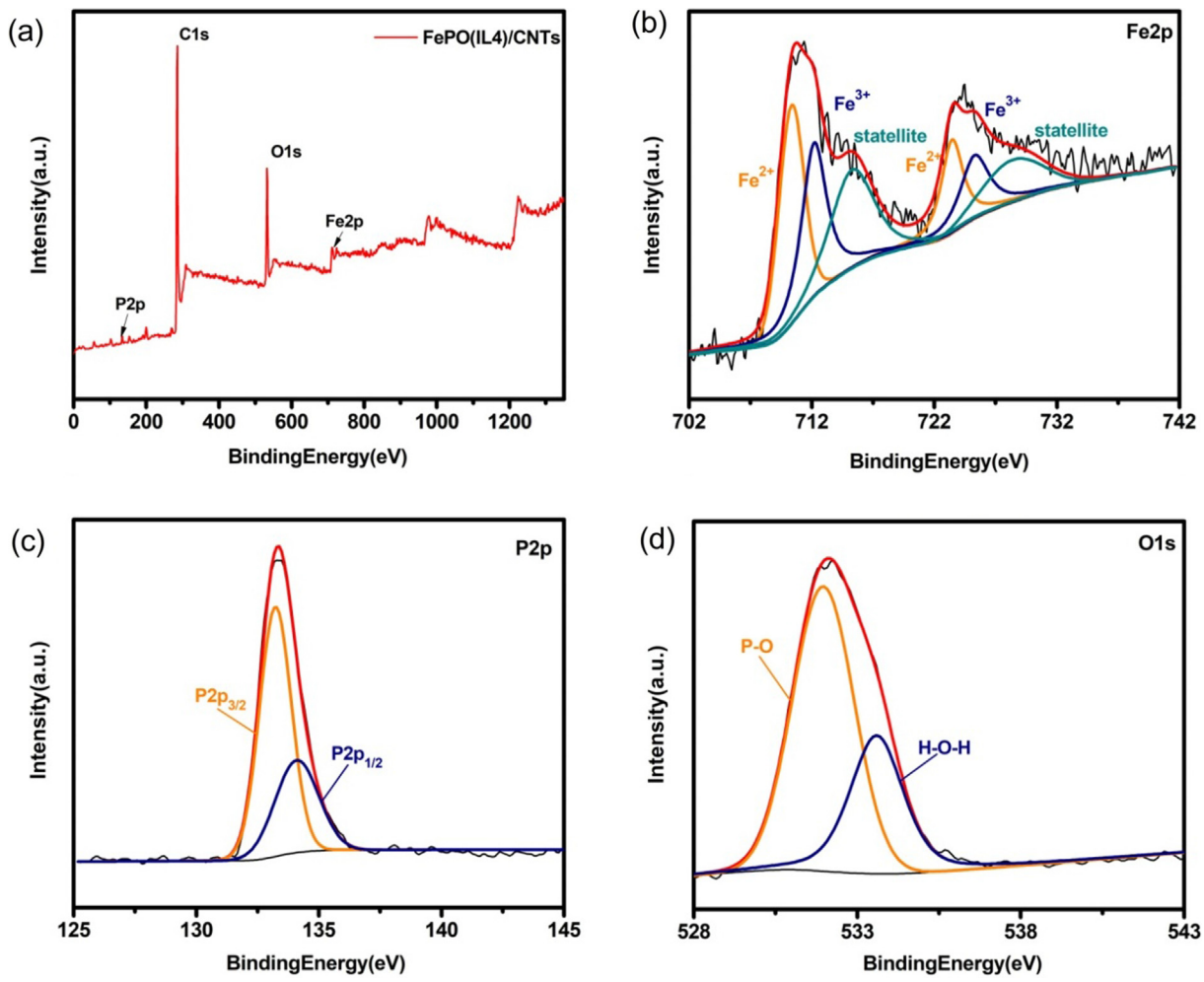

Fig. 3 **(a):** XPS spectra of FePO(IL4)/CNTs. **(b):** Fe 2p XPS spectra of FePO(IL4)/CNTs. **(c):** P 2p XPS spectra of FePO(IL4)/CNTs. **(d):** O 1 s XPS spectra of FePO(IL4)/CNTs.

iron phosphate nanostructures instead of bulky iron phosphate. Moreover, the Tafel curves of these materials were investigated and the Tafel slopes were obtained *via* fitting the corresponding LSV plots Fig. 4b).The Tafel slope of FePO (IL4)/CNTs was approximately 30 mV dec^{-1}, so the HER process occurred *via* the Volmer-Tafel mechanism, in which the recombination of adsorbed hydrogen was the rate-limiting step (Li et al., 2018).FePO(IL6)/CNTs shows a Tafel slope of 44.6 mV dec^{-1},implying the mechanism of FePO(IL6)/CNTs could be the Volmer-Heyrovsky reaction and the electrochemical desorption(Heyrovsky step)was a rate-limiting step. This low Tafel slope of FePO(IL4)/CNTs demonstrates a low energy barrier of hydrogen desorption and has better kinetics of hydrogen evolution.

Besides the good HER activity, these as-prepared catalysts also can be served as remarkable OER electrocatalysts. The OER electrocatalytic performance of as-prepared catalysts was analyzed in 1 M KOH solution.RuO_2 was applied as electrocatalyst for comparison. TheFig.5a displays the polarization curves of as-prepared catalysts, the FePO(IL4)/CNTs shows the best OER electrocatalytic performance and has the lowest onset potential of 1.48 V. And FePO(IL4)/CNTs needs 300 mV to obtain the current density of 10 mA cm^{-2}, which is superior to FePO(IL6)/CNTs, FePO(IL4), CNTs and RuO_2. In addition, the catalytic performance of FePO (IL4)/CNTs is comparable with other transition metal-based catalysts (Table S1). The OER electrocatalytic performance of FePO(IL4)/CNTs and FePO(IL6)/CNTs is better than FePO(IL4) and CNTs, showing the same trend as HER performance. The OER kinetics was investigated *via* Tafel slopes of catalysts (Fig. 5b). The Tafel slope for FePO(IL4)/CNTs (73.3 mV dec^{-1}) is much lower than FePO(IL6)/CNTs(74.8 $mVdec^{-1}$), FePO(IL4)(84.7 $mVdec^{-1}$), CNTs(138.5 $mVdec^{-1}$) and RuO_2(77.3 $mVdec^{-1}$), indicating the FePO(IL4)/CNTs displays more favorable OER kinetics.

To further evaluate the catalytic performance, electrochemical surface area (ECSA) and electrochemical impedance spectroscopy (EIS) of these catalysts were studied. The value of ECSA is closely related to the double-layer capacitance (C_{dl}), which was utilized to investigate the catalytically active sites of catalysts (Huang et al., 2019; Yang et al., 2018; Yu et al., 2016). Moreover, C_{dl} is proportional to ECSA (, xxxx). Herein, cyclic voltammetry (CV) was used to estimate the ECSA values under different scan rates in the non-Faraday region of 0.06 $\sim$ 0.16 V for HER and 0 $\sim$ 0.2 V for OER. There was no redox reaction and charge transfer in the selected voltage range, thus

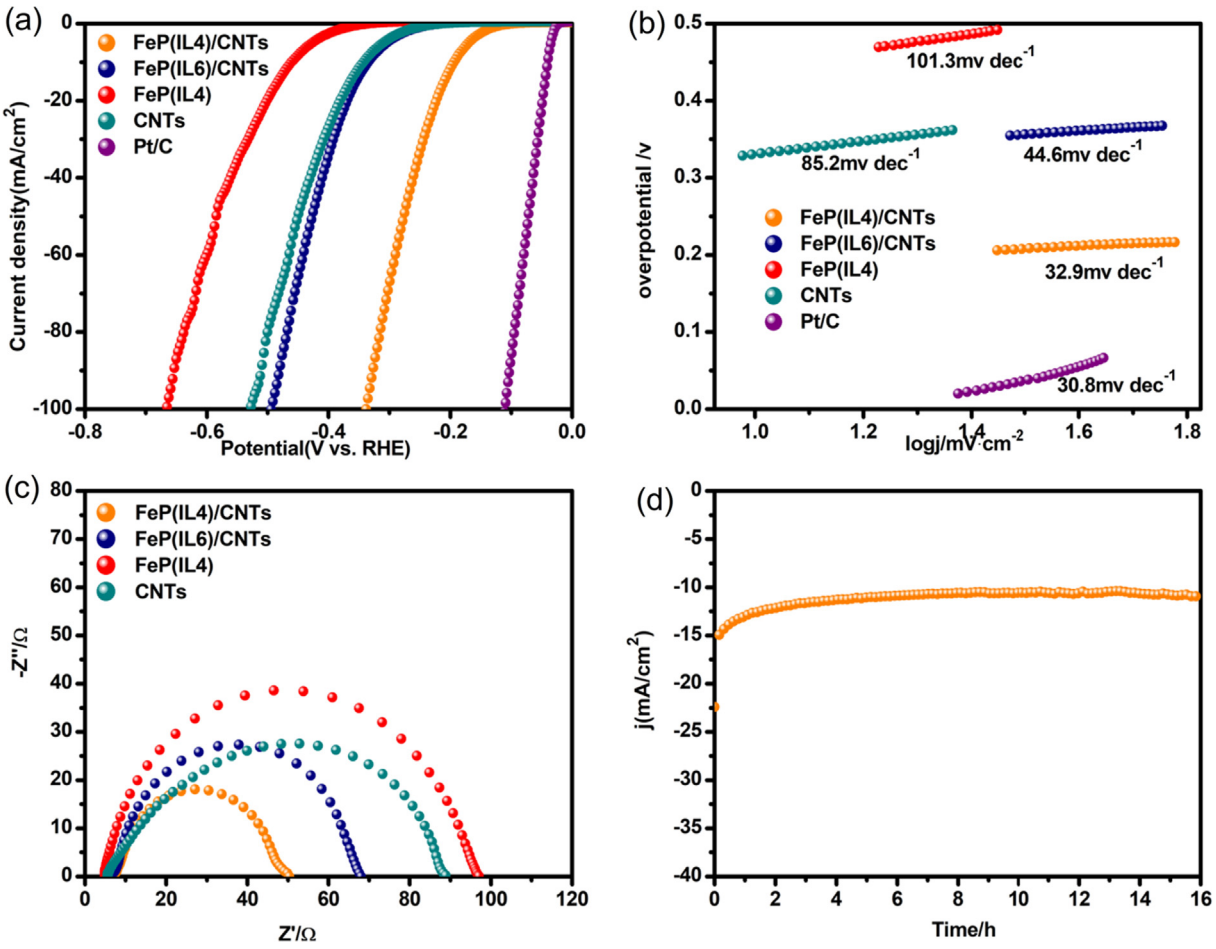

Fig. 4 **(a)**: Linear sweep voltammograms of prepared catalysts; **(b)**: Tafel plots for HER using prepared catalyst. **(c)**: Electrochemical impedance spectroscopy data for prepared catalysts. Data was collected for the electrode under HER overpotential: 550 mV. **(d)**: Time dependence of cathodic current density during electrolysis over 25 h at overpotential of 500 mV. FePO(IL4)/CNTs (orange), FePO(IL6)/CNTs (navy), FePO(IL4) (red), pristine CNTs (dark cyan) and Pt/C (purple) Catalyst loading amount: 50 μg. Electrolyte: 0.5 M H_2SO_4. IL to CNTs ratio: 5:1.

the current only was generated from double-layer charging and discharging (Yang et al., 2018; Amorim et al., 2020). As illustrated in Fig. S5, the C_{dl} of FePO(IL4)/CNTs was significantly higher than that of other catalysts for HER and OER, manifesting FePO(IL4)/CNTs possessed more effective active sites to promote the adsorption and desorption processes. Therefore, the catalytic performance of FePO(IL4)/CNT had been significantly improved. Furthermore, FePO(IL4)/CNTs exhibited the smallest faradaic impedance for HER and OER in Fig. 4c and Fig. 5c. The addition of CNTs can effectively reduce the Faraday impedance and improve the electron transfer ability, enhancing the catalytic kinetics. Thus, CNTs play an important role in forming iron phosphate nanoparticles and improving catalytic activity.

The catalytic stability of FePO(IL4)/CNTs was investigated by current–time (i-t) measurement. For the HER, the stability measurement was conducted with a constant over overpotential of500 mV for 25 h, and the stability measurement was conducted with a constant overpotential of 800 mV for 16 h for OER. As shown in Fig. 4d and Fig. 5d, the current density of FePO(IL4)/CNTs was barely changed, exhibiting excellent stability. Thus, FePO(IL4)/CNTs can be used as an effective and stable HER and OER electrocatalyst.

FePO(IL4)/CNTs was optimized in terms of microwave radiation time and IL/CNTs ratio. The ratio of IL to CNTs was adjusted from 1:1 to 15:1. It can be found that the optimal ratio is 5:1(Fig. S6). One possible reason is that the low ratio of IL/CNTs can not generate enough FePO(IL4)/CNTs, while a high ratio of IL/CNTs could prepare some extra FePO(IL4) that makes the catalytic performance poor. Then, the microwave radiation time was increased from 2 to 6 min. The results show that FePO(IL4)/CNTs has the best catalytic performance when the microwave irradiation time was 4 min(Fig. S7). A short radiation time can not obtain the iron phosphate completely, while prolonging the time of microwave irradiation would not significantly change the catalytic performance. To save the energy an time, the catalyst was prepared by microwave irradiation in 4 min.

4. Conclusions

In this study, ionic liquids were used as the dual-source of Fe and P to prepare iron phosphate through microwave radiation. These prepared iron phosphate/CNTs composites were used as electrocatalyst for water splitting, and IL can influence the

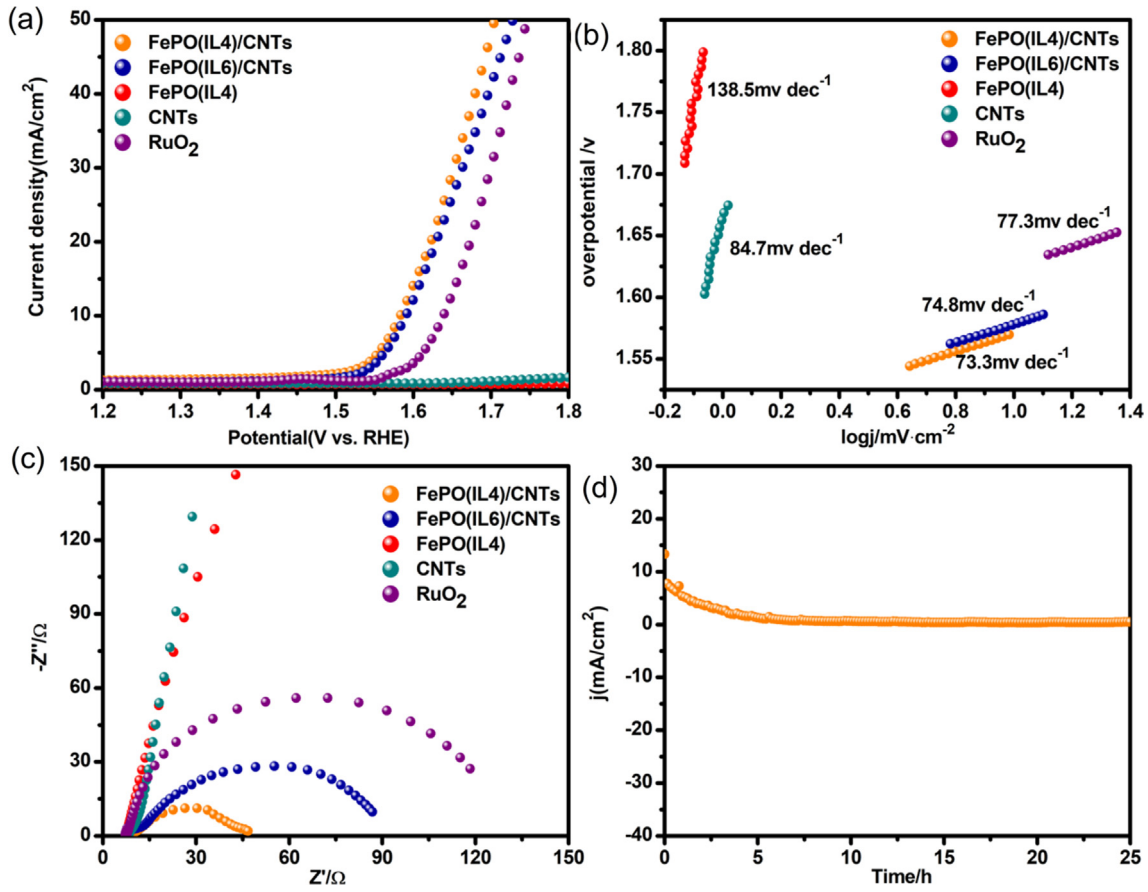

Fig. 5 **(a):** Linear sweep voltammograms of the catalysts for the OER.**(b)**: Tafel plots for OER using prepared catalysts; **(c)**: Electrochemical impedance spectroscopy data for prepared catalysts. Data was collected for the electrode under OER overpotential: 650 mV. **(d)**: Time dependence of cathodic current density during electrolysis over 16 h at overpotential of 800 mV. FePO(IL4)/CNTs (orange), FePO(IL6)/CNTs (navy), FePO(IL4) (red), pristine CNTs (dark cyan) and Ru_2O (purple). Catalyst loading amount: 50 μg. Electrolyte: 1 M KOH. IL to CNTs ratio: 5:1.

morphology of iron phosphate and electrocatalytic performance of these materials. In these catalysts, $Fe_7(PO_4)_6$/CNTs (FePO(IL4)/CNTs) generated from $[P(C_4H_9)_4][FeCl_4]$/CNTs exhibited excellent catalytic activity and stability for HER and OER. Moreover, CNTs not only contributed to the formation of iron phosphate nanoparticles, but also increased the conductivity of the catalyst, ameliorating the catalytic performance. Therefore, this method of microwave radiation using IL provide a simple, facile and eco-friendly strategy for transition metal phosphate, which possesses a good application prospect in other electrochemical research.

Declaration of Competing Interest

The authors declare that they have no known competing financial interests or personal relationships that could have appeared to influence the work reported in this paper.

Acknowledgements

This work is financially supported by the National Natural Science Foundation of China (No. 21902105) and the Open Fund of Guangdong Provincial Key Laboratory of Advanced Energy Storage Materials, South China University of Technology (AESM202108).

Appendix A. Supplementary data

Supplementary data to this article can be found online at https://doi.org/10.1016/j.arabjc.2021.103440.

References

Turner, J.A., 2004. Sustainable hydrogen production. Science 305 (5686), 972–974.

Schlapbach, L., 2009. Technology hydrogen-fuelled vehicles. Nature 460 (7257), 809–811.

Coughlin, R.W. et al, 1979. Hydrogen production from coal, water and electrons. Nature 279, 301–303.

Karunadasa, H.I., et al.2010.A molecular molybdenum-oxo catalyst for generating hydrogen from water.Nature.464:1329-1333.

Yang, C., Lei, H., Zhou, W.Z., Zeng, J.R., Zhang, Q.B., Hua, Y.X., Xu, C.Y., 2018. Engineering nanoporous Ag/Pd core/shell interfaces with ultrathin Pt doping for efficient hydrogen evolution reaction over a wide pH range. J. Materials Chemistry A. 6 (29), 14281–14290.

Wang, J., Xu, F., Jin, H., Chen, Y., Wang, Y., 2017. Non-Noble Metal-based Carbon Composites in Hydrogen Evolution Reaction:

Fundamentals to Applications. Adv. Mater. 29 (14), 1605838. https://doi.org/10.1002/adma.v29.1410.1002/adma.201605838.

Sun, H., Yan, Z., Liu, F., Xu, W., Cheng, F., Chen, J., 2020. Self-Supported Transition-Metal-Based Electrocatalysts for Hydrogen and Oxygen Evolution. Adv. Mater. 32 (3), 1806326. https://doi.org/10.1002/adma.v32.310.1002/adma.201806326.

Li, Y., Dong, Z., Jiao, L., 2020. Multifunctional Transition Metal-Based Phosphides in Energy-Related Electrocatalysis. Advanced Energy Materials. 10 (11), 1902104. https://doi.org/10.1002/aenm.v10.1110.1002/aenm.201902104.

Shi, Y., Zhang, B.2016.Recent advances in transition metal phosphide nanomaterials: synthesis and applications in hydrogen evolution reaction.Chem Soc Rev.45:1529-1541.

Callejas, J.F., Read, C.G., Popczun, E.J., McEnaney, J.M., Schaak, R. E., 2015. Nanostructured Co_2P Electrocatalyst for the Hydrogen Evolution Reaction and Direct Comparison with Morphologically Equivalent CoP. Chem. Mater. 27 (10), 3769–3774.

Pu, Z., Amiinu, I.S., Zhang, C., Wang, M., Kou, Z., Mu, S., 2017. Phytic acid-derivative transition metal phosphides encapsulated in N, P-codoped carbon: an efficient and durable hydrogen evolution electrocatalyst in a wide pH range. Nanoscale. 9 (10), 3555–3560.

Yao, Y., Mahmood, N., Pan, L., Shen, G., Zhang, R., Gao, R., Aleem, F.-e., Yuan, X., Zhang, X., Zou, J.-J., 2018. Iron phosphide encapsulated in P-doped graphitic carbon as efficient and stable electrocatalyst for hydrogen and oxygen evolution reactions. Nanoscale. 10 (45), 21327–21334.

Yu, F., et al.2018.High-performance bifunctional porous non-noble metal phosphide catalyst for overall water splitting.Nat Commun.9:2551.

Ryu, J., et al.2015.In Situ Transformation of Hydrogen-Evolving CoP Nanoparticles: Toward Efficient Oxygen Evolution Catalysts Bearing Dispersed Morphologies with Co-oxo/hydroxo Molecular Units.ACS Catalysis.5:4066-4074.

Ülker, E.2019.Hydrothermally Synthesized Cobalt Borophosphate as an Electrocatalyst for Water Oxidation in the pH Range from 7 to 14.ChemElectroChem.6:3132-3138.

Liang, Q., Zhong, L., Du, C., Luo, Y., Zhao, J., Zheng, Y., Xu, J., Ma, J., Liu, C., Li, S., Yan, Q., 2019. Interfacing Epitaxial Dinickel Phosphide to 2D Nickel Thiophosphate Nanosheets for Boosting Electrocatalytic Water Splitting.ACS. NANO 13 (7), 7975–7984.

Zhong, D., Liu, L., Li, D., Wei, C., Wang, Q., Hao, G., Zhao, Q., Li, J., 2017. Facile and fast fabrication of iron-phosphate supported on nickel foam as a highly efficient and stable oxygen evolution catalyst.Journal of. Materials Chemistry A. 5 (35), 18627–18633.

Zhang, B., Xue, Y., Jiang, A., Xue, Z., Li, Z., Hao, J., 2017. Ionic Liquid as Reaction Medium for Synthesis of Hierarchically Structured One-Dimensional MoO_2 for Efficient Hydrogen Evolution.ACS Applied Materials &. Interfaces. 9 (8), 7217–7223.

Khalate, S.A., Kadam, S.A., Ma, Y.-R., Pujari, S.S., Marje, S.J., Katkar, P.K., Lokhande, A.C., Patil, U.M., 2019. Hydrothermally synthesized Iron Phosphate Hydroxide thin film electrocatalyst for electrochemical water splitting. Electrochim. Acta 319, 118–128.

Read, C.G., Callejas, J.F., Holder, C.F., Schaak, R.E., 2016. General Strategy for the Synthesis of Transition Metal Phosphide Films for Electrocatalytic Hydrogen and Oxygen Evolution. ACS Appl. Mater. Interfaces 8 (20), 12798–12803.

Wang, J., Cui, W., Liu, Q., Xing, Z., Asiri, A.M., Sun, X., 2016. Recent Progress in Cobalt-Based Heterogeneous Catalysts for Electrochemical Water Splitting. Adv. Mater. 28 (2), 215–230.

Pan, Y., Liu, Y., Zhao, J., Yang, K., Liang, J., Liu, D., Hu, W., Liu, D., Liu, Y., Liu, C., 2015. Monodispersed nickel phosphide nanocrystals with different phases: synthesis, characterization and electrocatalytic properties for hydrogen evolution.Journal of. Materials Chemistry A. 3 (4), 1656–1665.

Wang, J., Wang, J., Zhang, M., Li, S., Liu, R., Li, Z., 2020. Metal-organic frameworks-derived hollow-structured iron-cobalt bimetallic phosphide electrocatalysts for efficient oxygen evolution reaction. J. Alloy. Compd. 821, 153463. https://doi.org/10.1016/j.jallcom.2019.153463.

Liu, M., et al.2017.Fe2P/reduced graphene oxide/Fe2P sandwich-structured nanowall arrays: a high-performance non-noble-metal electrocatalyst for hydrogen evolution.Journal of Materials Chemistry A.5:8608-8615.

Suliman, M.H., Adam, A., Siddiqui, M.N., Yamani, Z.H., Qamar, M., 2019. Facile synthesis of ultrathin interconnected carbon nanosheets as a robust support for small and uniformly-dispersed iron phosphide for the hydrogen evolution reaction. Carbon 144, 764–771.

Kozlyakova, E., Danilovich, I., Volkov, A., Zakharov, K., Dimitrova, O., Belokoneva, E., Shvanskaya, L., Zvereva, E., Chareev, D., Volkova, O., Vasiliev, A., 2018. Tuning of physical properties of $Fe_7(PO_4)_6$ by sodium intercalation. J. Alloy. Compd. 744, 600–605.

Fan, H.-H., Li, H.-H., Wang, Z.-W., Li, W.-L., Guo, J.-Z., Fan, C.-Y., Sun, H.-Z., Wu, X.-L., Zhang, J.-P., 2019. Tailoring Coral-Like Fe_7Se_8@C for Superior Low-Temperature Li/Na-Ion Half/Full Batteries: Synthesis, Structure, and DFT Studies. ACS Appl. Mater. Interfaces 11 (51), 47886–47893.

Zhao, D., et al.2018.N-Doped carbon shelled bimetallic phosphates for efficient electrochemical overall water splitting.Nanoscale.10:22787-22791.

Yuan, C.-Z., Jiang, Y.-F., Wang, Z., Xie, X., Yang, Z.-K., Yousaf, A. B., Xu, A.-W., 2016. Cobalt phosphate nanoparticles decorated with nitrogen-doped carbon layers as highly active and stable electrocatalysts for the oxygen evolution reaction.Journal of. Materials Chemistry A. 4 (21), 8155–8160.

Li, J., Xu, W., Zhou, D., Luo, J., Zhang, D., Xu, P., Wei, L., Yuan, D., 2018. Synthesis of 3D flower-like cobalt nickel phosphate grown on Ni foam as an excellent electrocatalyst for the oxygen evolution reaction. J. Mater. Sci. 53 (3), 2077–2086.

Xu, J., Xiong, D., Amorim, I., Liu, L., 2018. Template-Free Synthesis of Hollow Iron Phosphide-Phosphate Composite Nanotubes for Use as Active and Stable Oxygen Evolution Electrocatalysts.ACS. Applied Nano Materials. 1 (2), 617–624.

Yang, L., Guo, Z., Huang, J., Xi, Y., Gao, R., Su, G.e., Wang, W., Cao, L., Dong, B., 2017. Vertical Growth of 2D Amorphous $FePO_4$ Nanosheet on Ni Foam: Outer and Inner Structural Design for Superior Water Splitting. Adv. Mater. 29 (46), 1704574. https://doi.org/10.1002/adma.v29.4610.1002/adma.201704574.

Huang, S., Meng, Y., Cao, Y., He, S., Li, X., Tong, S., Wu, M., 2019. O- and P-doped hollow carbons: Metal-free bifunctional electrocatalysts for hydrogen evolution and oxygen reduction reactions. Appl. Catal. B 248, 239–248.

Yang, L., Zhang, L.i., Xu, G., Ma, X., Wang, W., Song, H., Jia, D., 2018. Metal–Organic-Framework-Derived Hollow CoSx@MoS_2 Microcubes as Superior Bifunctional Electrocatalysts for Hydrogen Evolution and Oxygen Evolution Reactions. ACS Sustainable Chem. Eng. 6 (10), 12961–12968.

Yu, L., Xia, B.Y., Wang, X., Lou, X.W., 2016. General Formation of M-MoS_3 (M = Co, Ni) Hollow Structures with Enhanced Electrocatalytic Activity for Hydrogen Evolution. Adv. Mater. 28 (1), 92–97.

Wang, C., et al.2020.Tailoring the nanostructure and electronic configuration of metal phosphides for efficient electrocatalytic oxygen evolution reactions.Nano Energy.69:104453

Amorim, I., et al.2019.Bi-metallic cobalt-nickel phosphide nanowires for electrocatalysis of the oxygen and hydrogen evolution reactions. Catalysis Today.358: 196-202